Organic Modification of Eutectogels enhances Electrolyte/Electrode contact in Sodium-Ion Batteries

Jonas Mercken,[a,b] Dries De Sloovere,*[a,b] Bjorn Joos,[a,b] Digvijay Ghogare,[a,c] Younas Verhille,[a] Sander Smeets,[a] Elien Derveaux,[a] Peter Adriaensens,[a] Marlies Van Bael[a,b] and An Hardy,[a,b]

[a] J. Mercken, D. De Sloovere, B. Joos, D. Ghogare, Y. Verhille, S. Smeets, E. Derveaux, P. Adriaensens, M. K. Van Bael, A. Hardy
Institute for Materials Research (imo-Imomec)
UHasselt and Imec, Agoralaan, building D, 3590 Diepenbeek, Belgium
E-mail: dries.desloovere@uhasselt.be

[b] J. Mercken, D. De Sloovere, B. Joos, M. K. Van Bael, A. Hardy
EnergyVille
Thor Park 8320, 3600 Genk, Belgium

[c] D. Ghogare
Electrochemistry Excellence Centre (ELEC)
Flemish Institute for Technological Research (VITO)
Boeretang 200, Mol, 2400 Belgium

Supporting information for this article is given via a link at the end of the document.

Abstract: Na^+ ion conducting deep eutectic solvents hold promise as alternative electrolytes for future sodium-ion batteries because of their higher thermal stability compared to conventional liquid electrolytes, drastically improving safety characteristics. However, their liquid nature remains to pose a risk of potential leakage. In this study, the latter is resolved by the encapsulation of deep eutectic solvents in a solid host matrix, creating so-called eutectogels, which are promising alternatives to ionogels because of their cost-effectiveness. The nature of the host matrix heavily influences the mechanical properties of the gels, where completely inorganic host materials readily experience mechanical deterioration when stress is applied. In this work, organic modification of the inorganic host matrix enhances the pliability of eutectogels, decreasing their Young's modulus from 4.8 to 2.1 MPa. This results in an improved electrode/electrolyte contact (reduced charge-transfer resistance) without compromising ionic conductivity (up to 0.17 mS cm^{-1}) or electrochemical stability window (~0.9 V vs. Na^+/Na to ~4.5 vs. Na^+/Na). As such, the eutectogels outperformed conventional liquid SIB electrolytes in full cells.

Introduction

The commercialization of sodium-ion batteries (SIBs) has marked the beginning of their role in complementing the decades-old lithium-ion battery (LIB) market.[1, 2] A SIB has a similar working principle as a LIB, but the charge carriers are Na^+ ions instead of Li^+ ions. The main driver for developing SIBs is their potential sustainable character and improved cost-effectiveness compared to LIBs.[3] SIBs are forecasted to cost 40-87 USD/kWh compared to 89-120 USD/kWh for LIBs.[4-6] The reduced price for SIBs can mainly be explained by the 1000 times higher abundance of Na compared to Li and the replacement of Cu with Al foil as anode current collector.[7, 8] Hard carbon (HC) and 'Prussian White,' ($Na_2Fe[Fe(CN)_6]$) a derivative of 'Prussian Blue,' are potential active negative and positive electrode materials for commercial SIBs, respectively.[9] SIB cells can deliver an energy density of 160 Wh kg^{-1}, forecasted to increase to 200 Wh kg^{-1} in the coming years, being competitive with low-cost LIBs based on LFP ($LiFePO_4$, 160 Wh kg^{-1}) but not with premium LIBs (250 Wh kg^{-1}).[10-12]

Another component vital for the commercialization of SIBs is the electrolyte. SIB electrolyte development follows similar trends as those seen with LIBs.[13, 14] Non-flammable electrolytes with solid properties are considered the holy grail to obtain batteries with record-breaking energy densities and enhanced safety. The increased energy density originates from their theoretically wider electrochemical stability window (ESW), potentially enabling electrochemical compatibility with both sodium metal and high-voltage positive electrode materials.[15] The minimal requirements for solid-like electrolytes are thermal, chemical, and electrochemical stability, in addition to non-flammability, high ionic conductivity, and optimized mechanical properties.[16, 17] Ionogels, which consist of an (ILE) encapsulated within a solid matrix, can meet all these requirements, even if ILEs are considered not to be cost-effective.[18, 19] Gels with a silica matrix (inorganic) have a higher thermal stability and ionic conductivity compared

to their polymer-based analogs, as we showed for lithium-ion conductors.[20, 21] In our previous work, the inorganic matrix of silica-based ionogels was organically modified with phenyl groups, effectively reducing their Young's moduli and improving the electrode/electrolyte contact.[22] Besides enhancing their flexibility, the organic modification resulted in pi-pi stacking between the ionic liquid cation and the phenyl moieties. This, in turn, led to the migration of hydrophilic anions to the bulk ILE, inducing the formation of large, immobile clusters and a lower ionic conductivity. Based on this observation, we hypothesize that the trade-off between pliability (i.e., low Young's modulus) and ionic conductivity may be overcome by substituting the ILE with a conductive liquid that cannot undergo pi-pi stacking, such as a deep eutectic solvent (DES).[23, 24]

Deep eutectic solvents (DESs) may be viable alternatives for ILEs, as they are cost-effective and generally do not contain any aromatic constituents. A DES is a mixture of a hydrogen bond donor (HBD) and a hydrogen bond acceptor (HBA) with a melting temperature below the predicted melting temperature based on their colligative properties.[25] In general, DESs offer the additional advantages of low vapor pressure, high conductivity, and non-flammability.[26] In the field of SIBs and in general, the use of DESs is still limited. An overview of various Na^+ conducting DESs for application in SIBs and supercapacitors (SCs) is given in Table 1. In our group's previous work, De Sloovere *et al*. developed a series of Na^+ ion conducting DESs based on NaTFSI (sodium bis(trifluoromethanesulfonyl)imide, HBA) and *N*-methyl acetamide (NMA, HBD), improving the anodic stability limit up to ~4.65 V vs. Na^+/Na by increasing the NaTFSI concentration.[23] The latter was likely caused by the replacement of hydrogen bonds between the NMA molecules by ion-dipole interactions between Na^+ ions and NMA. A different study by Liu *et al*. reported ionic conductivity values up to 23.8 mS cm^{-1} for a 'water-locked' succinonitrile (SN)-$NaClO_4$-H_2O-based DES.[27] Here, the high ionic conductivity was partly caused by the water molecules. However, the latter were not electrochemically active due to the strong interaction with succinonitrile. Remarkably, the cathodic stability limit of most of the DES for SIBs lies well above 1 V vs. Na^+/Na, making it necessary to avoid Na metal as negative electrode. To address this limitation, Kelchtermans *et al*. developed a DES based on NaFSI (sodium bis(fluorosulfonyl)imide) and NMA, which showed compatibility with Na metal.[24] To the best of our knowledge, there are thus far no reports of gel electrolytes consisting of encapsulated DESs (termed 'eutectogels') being used in SIBs.[20]

Table 1. Overview of deep eutectic solvents (DESs) used in sodium-ion batteries (SIBs) or supercapacitors (SCs). NaTFSI: sodium bis(trifluoromethanesulfonyl)imide, NMA: N-methyl acetamide, NaFSI: sodium bis(fluorosulfonyl)imide, DMIm: dimethyl imidazolium, SN: succinonitrile, NaFTFSI: sodium (fluorosulfonyl)(trifluoromethanesulfonyl)imide, NaTFSICN: sodium cyanotrifluoromethanesulfonyl)imide, EC: ethylene carbonate, FMD: formamide, RT: room temperature. '/': not reported in study.

Composition	Ionic conductivity (mS cm^{-1})	Thermal stability (°C)	Cathodic stability (V vs. Na^+/Na)	Anodic stability (V vs. Na^+/Na)	Application	Ref.
NaTFSI/NMA	0.355 (20 °C)	100	/	~4.65	SIB	[23]
NaFSI/NMA	0.056 (20 °C)	150	~0	~4.0	SIB	[24]
SN-$NaClO_4$-H_2O	23.8 (25 °C)	/	~1.25	~4.6	SIB	[27]
NaTFSI/NMA	/	/	/	/	SIB	[28, 29]
NaFSI/DMIm	1.53 (28 °C)	350-375	~1.7	~4.9	SIB	[30]
NaFTFSI or NaTFSICN with EC	7.48 or 5.46 (25 °C)	/	/	/	SC	[31]
$NaNO_3$/FMD	14.01 (RT)	/	~1.6	~4.7	SC	[32]

In this study, we report the first application of eutectogels as electrolytes in SIBs. As these materials do not contain aromatic constituents, the previously observed trade-off between mechanical properties and ionic conductivity can be successfully circumvented by avoiding the mechanism of pi-pi stacking. Moreover, organic modification simultaneously improves electrode/electrolyte contact and increases ionic conductivity. The organic modification does not negatively influence the eutectogels' electrochemical stability windows (ESWs). The holistic improvement in functional properties is underpinned by a detailed investigation of the molecular interactions occurring within the eutectogels. Full cells containing eutectogels with more organic modification are shown to have a high electrochemical stability and lower charge transfer resistance. As such, organically modified eutectogels are shown to be viable electrolyte alternatives for the future development of all-solid-state SIBs.

Results and Discussion

Eutectogel monoliths were synthesized by encapsulating a DES in a solid matrix. Full synthetic details are given in the Supporting Information, Figure S1, Figure S2, and Table S1, which give an overview of the chemical reactions releasing water during silica condensation, show the casings used for eutectogel drying, and the weighed amounts

and volumes for the preparation of eutectogels, respectively. As liquid DES electrolyte, we specifically chose NaTFSI/NMA in a molar ratio of 3/7 for its high anodic stability (~4.65 V vs. Na^+/Na) and workable ionic conductivity of 0.355 mS cm^{-1} (20 °C).[23] An overview of the organically modified, silica-based eutectogels, their compositions, and their (physico)chemical properties can be found in Table 2. All eutectogel monoliths were homogeneous, transparent, and self-standing. The percentage of organically modified silane was fixed at 25% PhTMS and 12.5% DPhDMS to maintain equal molar amounts of phenyl groups in the eutectogels. PhTMS and DPhDMS contain one phenyl and three methoxy moieties resp. two phenyl and two methoxy moieties. The methoxy moieties will hydrolyze and condensate to form Si-O-Si bridges, but the phenyl group(s) will remain behind in the organically modified silica matrix. Therefore, with 25% PhTMS and 12.5% DPhDMS, the same amount of phenyl groups will be left behind in the matrix after the hydrolysis/condensation process is finished. PhTMS contains one phenyl moiety and three methoxy moieties per molecule. The methoxy moieties can undergo hydrolysis and condensation, resulting in a solid and branched interconnected structure. DPhDMS only contains two methoxy groups. As such, each DPhDMS molecule can only covalently bond to two other alkoxysilane molecules, which will result in a less interconnected solid structure. Therefore, the resulting DPhDMS-based eutectogels are still expected to have a less rigid network and to be more flexible than those based on PhTMS (in spite of their equal phenyl content).

Table 2. Overview of the (organically modified) eutectogels, their compositions, ionic conductivities, and Young's moduli. The first part of the sample nomenclature (e.g., 25PhTMS_0.75) states the Si molar percentage of TEOS replaced by organically modified silanes. In this example, 25PhTMS contains 25 Si molar% of PhTMS and 75 Si molar% of TEOS. The number _0.75 states the molar ratio of NMA/total Si and is a measure for the amount of liquid DES in the eutectogels. A higher number means more NMA; thus, more DES is present in the eutectogels. A formic acid (FA) over Si molar ratio of 2 was used to induce the hydrolysis and condensation of the silica precursors. Ionic conductivity was measured at 20 °C, with standard deviation over 3 samples between brackets. Young's modulus was measured using compression tests, with standard deviation over 3 samples between brackets. '/' means not applicable.

Sample	Si molar% of organically modified silane	Si molar% of TEOS	NMA/Si molar ratio	Ionic conductivity (20 °C) (mS cm^{-1})	Young's modulus (MPa)
DES	/	/	/	0.355 [19]	/
100TEOS_0.75	0	100	0.75	0.0034 (± 0.0002)	44 (± 1)
100TEOS_1.00			1.00	0.0103 (± 0.0004)	43.2 (± 0.3)
100TEOS_1.50			1.50	0.034 (± 0.001)	37 (± 2)
100TEOS_2.00			2.00	0.075 (± 0.005)	36 (± 2)
100TEOS_3.00			3.00	0.124 (± 0.001)	10.1 (± 0.1)
100TEOS_4.00			4.00	0.16 (± 0.01)	4.8 (± 0.2)
25PhTMS_0.75	25	75	0.75	0.0033 (± 0.0003)	36 (± 1)
25PhTMS_1.00			1.00	0.016 (± 0.001)	38.2 (± 0.8)
25PhTMS_1.50			1.50	0.045 (± 0.001)	27 (± 1)
25PhTMS_2.00			2.00	0.101 (± 0.003)	12 (± 2)
25PhTMS_3.00			3.00	0.126 (± 0.002)	4.2 (± 0.1)
25PhTMS_4.00			4.00	0.171 (± 0.007)	2.1 (± 0.1)
12.5DPhDMS_0.75	12.5	87.5	0.75	0.00150 (± 0.00009)	36 (± 1)
12.5DPhDMS_1.00			1.00	0.0089 (± 0.0005)	32.8 (± 0.7)
12.5DPhDMS_1.50			1.50	0.054 (± 0.001)	23.6 (± 0.4)
12.5DPhDMS_2.00			2.00	0.093 (± 0.006)	13.8 (± 0.8)

Mechanical and thermal properties

The Young's moduli (*E*) of the (organically modified) eutectogels were determined with compression tests (Figure 1). At equal DES content, eutectogels without organic modification have the highest *E* (i.e., have the highest stiffness). Organically modifying the silica matrix with phenyl groups replaces part of the alkoxy groups with non-hydrolyzing phenyl groups, resulting in the formation of a less rigid network and to a reduction in stiffness (Young's modulus). This reduction in Young's modulus is, for some samples, even more pronounced for DPhDMS-modified eutectogels (for instance, 100TEOS_1.50, 25PhTMS_1.50, and 12.5DPhDMS_1.50). This is likely caused by the fact that DPhDMS contains two alkoxy groups, and will therefore lead to the formation of a less rigid network than PhTMS, which contains three alkoxy groups.[22] Other eutectogels (for instance, 25PhTMS_0.75 and 12.5DPhDMS_0.75, or 25PhTMS_2.00 and 12.5DPhDMS_2.00) have nearly equal *E* values, considering the standard deviation on the measurements. Increasing the amount of encapsulated DES results in a lower *E*. For instance, 100TEOS_4.00 (4.8 MPa) has an 88% lower stiffness than 100TEOS_0.75 (44 MPa). As eutectogels with lower *E* values are expected to more readily accommodate rough electrode topologies, eutectogels with more organic modification and higher DES content should have better interfacial contact. As an important metric for electrolyte safety, the thermal stability of the (organically modified) eutectogels was investigated by thermogravimetric analysis under dry air atmosphere. Figure 1 shows the thermal stability of the 25PhTMS-based eutectogels. The thermal stabilities of the 100TEOS and 12.5DPhDMS-based eutectogels can be found in Figure

S3. The thermal stability of the eutectogels is limited by the evaporation of NMA, which occurs around 120 °C as confirmed with TGA-FTIR in Figure S4 and Table S2. For the liquid DES electrolyte, NMA evaporation occurs around 105 °C, which implies that DES encapsulation induces molecular interactions with the solid matrix, resulting in increased thermal stability. The second mass loss step originates from the decomposition of the $TFSI^-$ anions at 420 °C (Figure S4), which agrees well with earlier studies.[33, 34] Organic modification does not affect the eutectogels' thermal stability limit. Still, the oxidation of the phenyl groups in the organically modified eutectogels can be observed between 500 and 650 °C (Figure 1, Figure S3, and Figure S4). The thermal behavior of the gels was further analyzed with differential scanning calorimetry (DSC), which is available in the Supporting Information in Figure S5. Table S3 gives the glass transition temperatures over the different heating cycles.

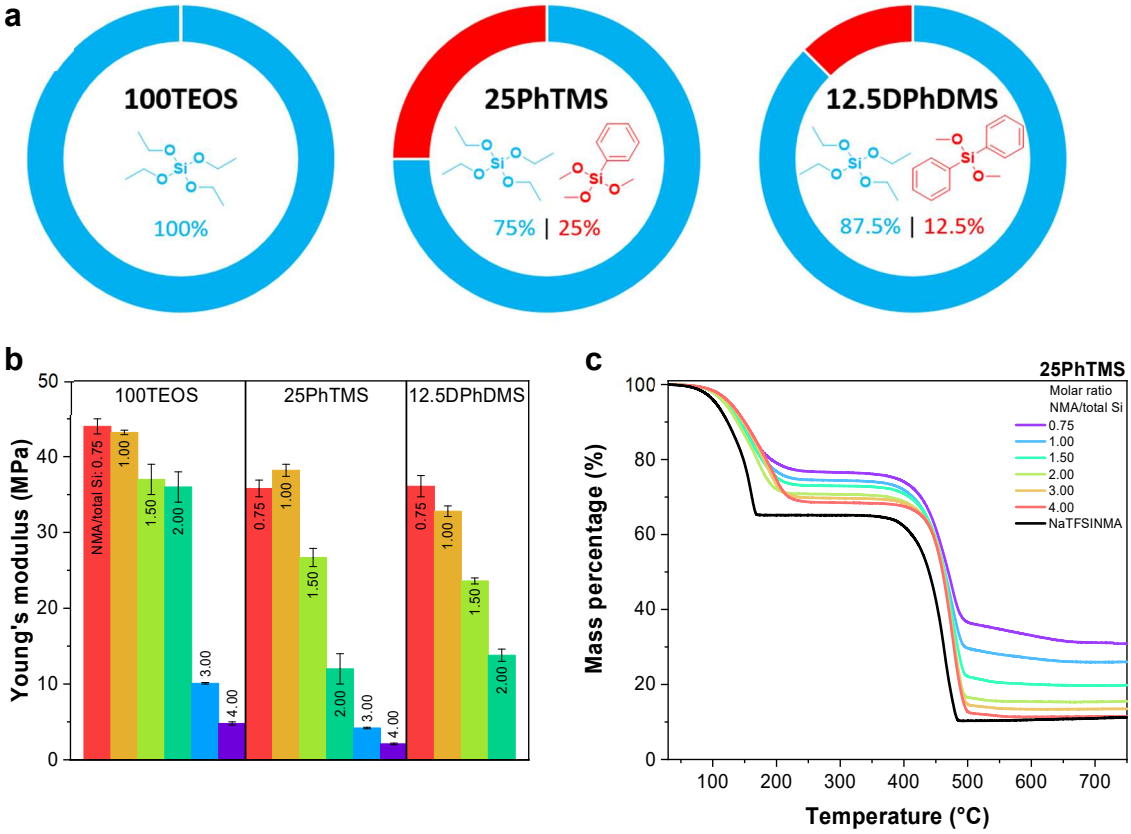

Figure 1. (a) Chemical structures of TEOS, PhTMS, and DPhDMS and their respective molar Si percentages. (b) Increasing the DES (NMA) content in the eutectogels and adding phenyl moieties into the silica matrix results in a decrease in Young's modulus. Error bars represent the standard deviation over 3 samples. (c) Thermal stability of eutectogels with PhTMS-modified silica matrices and of the DES. The thermal stabilities of the eutectogels are determined by the evaporation of the DES at approximately 120 °C (>5% weight loss). The $TFSI^-$ anions of the DES start to decompose at 420 °C. A higher DES-loading results in a lower residual weight. The oxidation of the phenyl groups is visible by the weight loss between 500 and 650 °C. TGA was measured under dry air atmosphere at 10 °C min^{-1}.

Ionic conductivity and electrochemical properties

The eutectogels' ionic conductivity values and electrochemical stability windows were measured after extensive drying (Figure 2). After the 50-day dry room (relative humidity <0.5%) drying stage, the majority of the volatiles (such as water, ethanol, and methanol, Figure S1) were removed, as determined by tracking the eutectogels' mass over time (Figure S6). The ionic conductivities in function of temperature can be fitted to the Vogel-Tammann-Fulcher (VTF) equation. VTF fitting parameters can be found in Table S4. The eutectogel conductivity at 20 °C increases with increasing DES content (Figure 2, Table 2), and none of them surpasses the conductivity of the liquid DES electrolyte (0.355 mS cm^{-1}).[23] Unlike previously reported ionogels,[22] organic modification does not result in a decrease in the ionic conductivity for the eutectogels reported in the study at hand. Instead, slight increases in conductivity can be observed, when comparing the ionic conductivity of 25PhTMS_2.00 (0.101 mS cm^{-1}) to that of 100TEOS_2.00 (0.075 mS cm^{-1}), where the latter does not have an organically modified solid matrix. In our previous work, the mechanical properties of an ionogel were improved by organically modifying its silica matrix with phenyl moieties. However, pi-pi stacking was observed between the aromatic phenyl groups of the silica matrix and the aromatic EMI^+ cations of the ILE, leading to a reduction in ionic conductivity with increasing extent of organic modification and effectively establishing a trade-off between mechanical properties and ionic conductivity.[22] In the study at hand, the DES used as the liquid component in the eutectogels does not contain aromatic compounds, implying that pi-pi stacking is impossible. This cancels the trade-off observed in organically modified ionogels, allowing a combination of both good mechanical properties and high ionic conductivity. Still, the

ionic conductivity and thermal stability observations suggest the existence of different ionic interactions occurring in the eutectogels (*vide infra*).

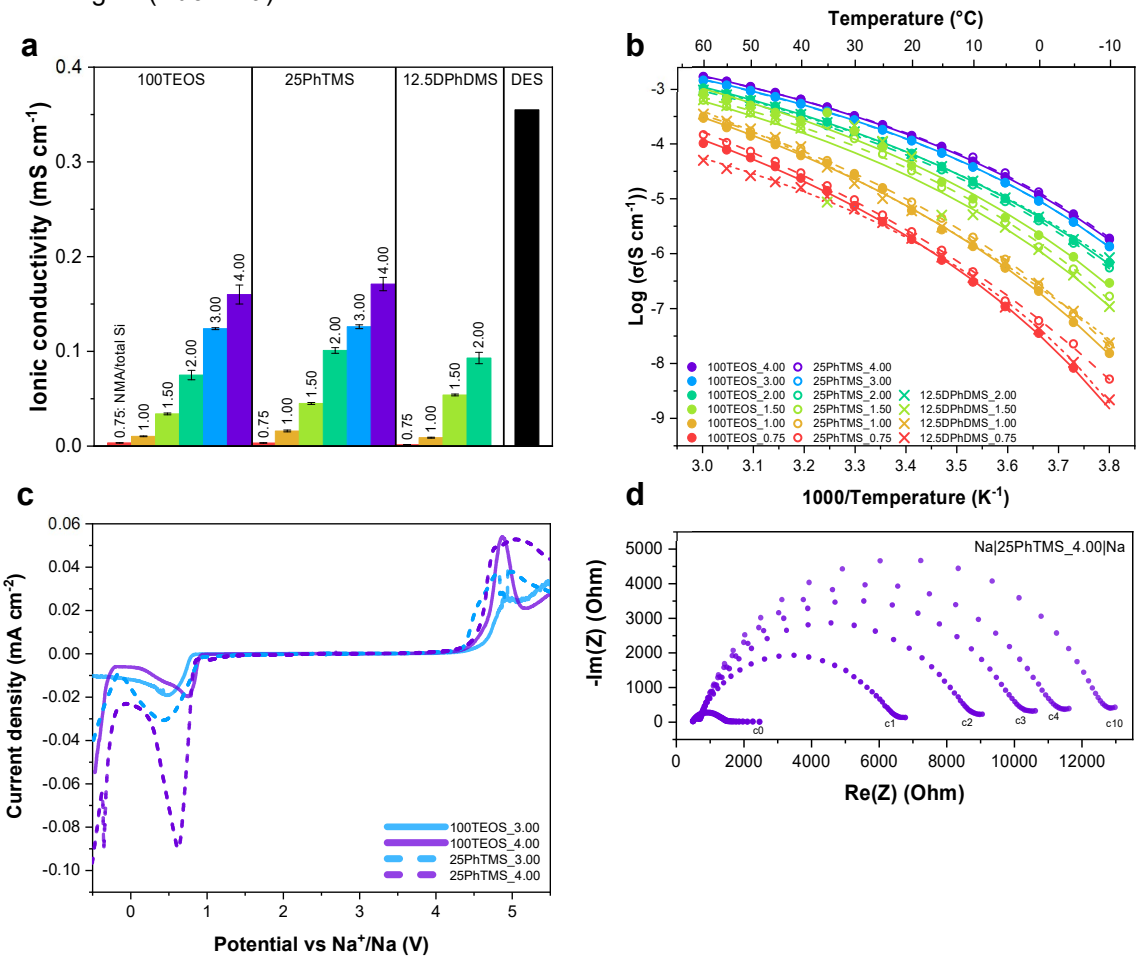

Figure 2. (a) The ionic conductivity is not affected by the presence of phenyl groups in the silica matrix in eutectogels. Ionic conductivity measured at room temperature (20 °C). Ionic conductivity increases with DES loading. Error bars represent the standard deviation over 3 samples. (b) Ionic conductivity in function of temperature. Solid and dotted lines represent VTF fitting. Fitting parameters can be found in the Supporting Information (Table S4). (c) Cathodic and anodic stabilities of 100TEOS_3.00 and 4.00, and 25PhTMS_3.00 and 4.00 measured with a three-electrode setup. Additional electrochemical stabilities can be found in Figure S7. (d) Nyquist plots of a Na|25PhTMS_4.00|Na symmetric cell showing an increasing semicircle (increasing charge transfer resistance), suggesting a resistive layer is being formed upon contact between Na metal and the eutectogel. One hour of OCV was applied to the cells between the EIS measurements.

The eutectogels' electrochemical stability windows (ESWs) are completely determined by the DES encapsulated in the eutectogels and can be found in Figure 2 and Figure S7. In other words, neither organic modification nor the DES loading negatively affects the eutectogels' stability. At high potentials (~4.5 V vs. Na^+/Na), the $TFSI^-$ anion starts to be oxidized, while at low potentials (~0.9 V vs. Na^+/Na), $TFSI^-$ anions and NMA are reduced.[21] This implies that these eutectogels can only be used in combination with negative electrode materials operating above 1 V vs. Na^+/Na. To elaborate this further, the stability of the eutectogels in contact with sodium metal was investigated. Symmetric Na|eutectogel|Na cells were made and subjected to EIS within regular time intervals (i.e., without ever passing current through the cell) (Figure 2, Figure S7). The charge transfer resistance significantly increases over the first ten hours after cell assembly, implying considerable reactivity between the eutectogel and sodium metal, Which causes the continuous deformation of the former. Similar incompatibility was previously observed for the stand-alone DES when in contact with sodium metal.[23] As such, the poor stability of the eutectogel/Na interface is caused by the reactivity of the DES.

Interactions between NaTFSI, NMA, H_2O, and the (organically modified) silica matrix

The interactions between the different chemical species (Na^+, $TFSI^-$, NMA, H_2O, silica, and phenyl moieties) were studied with ATR-FTIR, Raman, and solid-state NMR spectroscopy. The normalized ATR-FTIR spectra and the assignments of the absorption peaks can be found in Figure S8 and Table S5. Selected wavenumber regions of 25PhTMS samples, NaTFSI, and DES (NaTFSI/NMA) can be found in Figure 3. The most intense peak in the high wavenumber region (3500-3000 cm^{-1}, Figure S8) is the vibration peak at 3416 cm^{-1} from the N-H stretching of the NMA molecules hydrogen bonding with $TFSI^-$ anions.[35, 36] The O-H stretching peaks are also located in this region but are not clearly visible due to their weak intensity and the overlap with the amide A signals.[27] The stretch vibration of the carbonyl moiety of the 25PhTMS_0.75 and 25PhTMS_1.00 samples (1632 cm^{-1}, Figure 3a, shown

by the black arrow) shows a small red shift compared to the vibration wavenumber of DES (1645 cm^{-1}).[35-38] In the DES, the carbonyl functional group of NMA interacts with Na^+ ions. In the eutectogels, this interaction is replaced by the hydrogen bonding of the NMA carbonyl functional group with Si-OH moieties of the silica matrix and H_2O (*vide infra*). This change in the chemical environment is most pronounced for the eutectogels with low DES loading. The peak in samples with higher DES loadings (> 1.00 NMA/total Si molar ratio) show almost no red shift since the increased amount of DES results in a higher likelihood that Na^+ ions interact with NMA C=O moieties (more bulk-like). The C-N stretch and N-H bending vibration peak (1557 cm^{-1}, Figure 3a) do not shift upon confinement in a silica matrix.[36, 37] The DES ATR-FTIR spectra contain peaks relating to the in-plane vibration (1373 cm^{-1}), asymmetric stretch (1348 cm^{-1}), and out-of-plane vibration (1329 cm^{-1}) of the SO_2 group of the $TFSI^-$ anion (Figure 3b).[39, 40] These peaks are not shifted for the (organically modified) eutectogels, except for the eutectogels with the lowest DES-loadings (i.e., 25PhTMS_0.75 and 25PhTMS_1.00). The absorption peaks of 25PhTMS_0.75 and 25PhTMS_1.00 in this region (Figure 3b) can be considered as a superposition of the peaks of DES and NaTFSI salt. A similar observation can be made for the CF_3 stretch vibrations (1200 and 1186 cm^{-1} for NaTFSI salt and DES, respectively, Figure 3c) and for the peak at 800 cm^{-1} (NaTFSI salt) and 793 cm^{-1} (DES, Figure 3d).[39, 40] As such, the low-loaded Na-DES eutectogels appear to contain $TFSI^-$ anions in two different chemical environments. One resembles a liquid DES-like $TFSI^-$ anion, hydrogen bonding with NMA molecules in the bulk of the DES, and a second resembles a solid salt-like $TFSI^-$ anion. The presence of this solid salt-like $TFSI^-$ anion in _0.75 and _1.00 eutectogels might be one of the reasons for their very low ionic conductivities (< 0.02 mS cm^{-1}, Table 2). As NMA tends to coordinate to the silica matrix in these samples, the $TFSI^-$ anion concentration increases in the bulk of the DES, which, upon interaction with Na^+ ions, resembles a more solid salt-like character. Additional proof of the formation of salt-like TFSI is given in Figure S9. The above observations are also valid when the silica matrix is not organically modified. For the eutectogels containing higher amounts of DES, the salt-like $TFSI^-$ anions are not present, since only the signals of the liquid-like $TFSI^-$ anions appear in the FTIR spectra (Figure 3). Additionally, these high DES-loaded eutectogels contain relatively higher amounts of water (*vide infra*), making the presence of the salt-like $TFSI^-$ anions less likely. Raman spectroscopy results can be found in the Supporting Information in Figure S10.

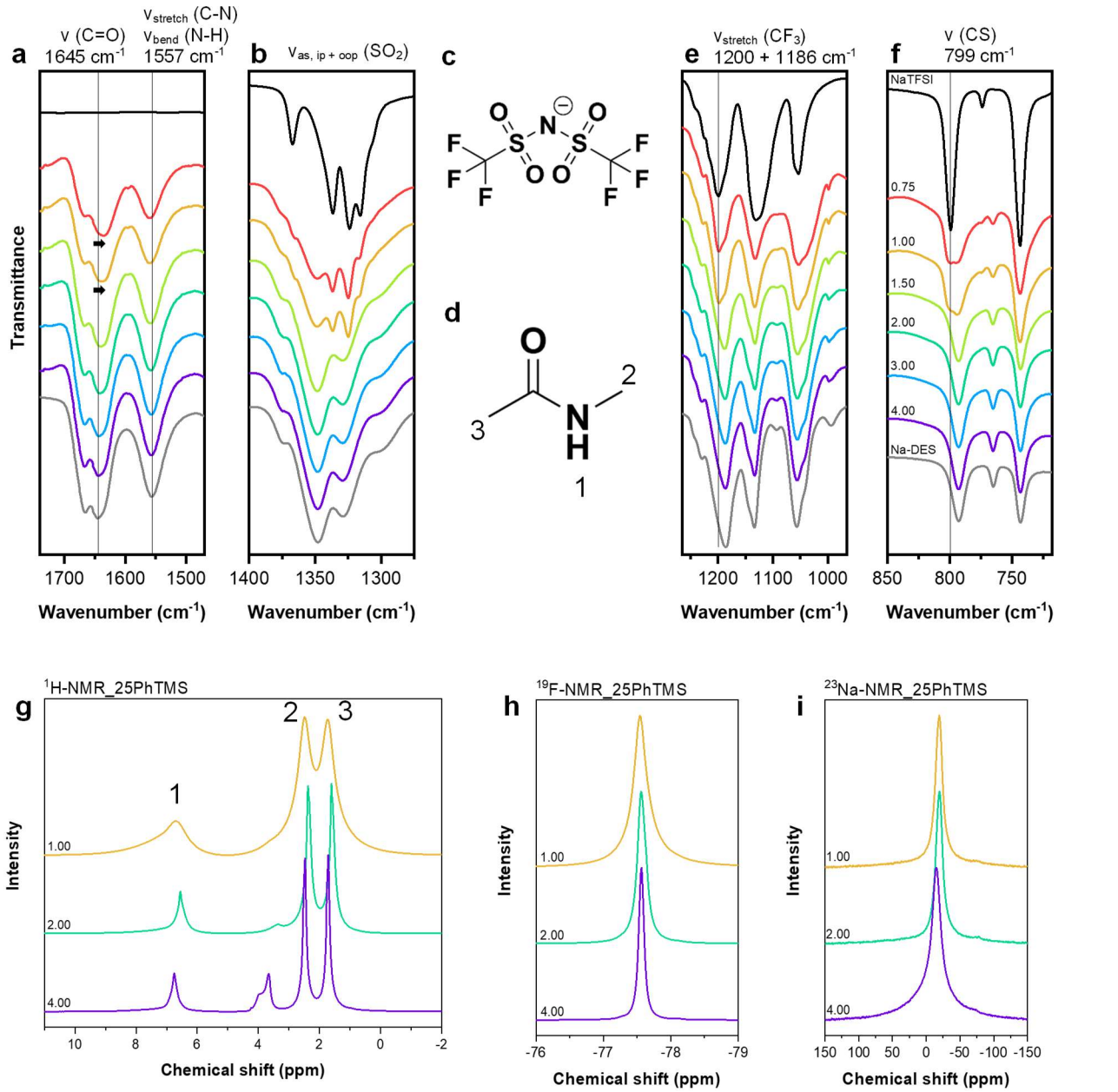

Figure 3. Normalized ATR-FTIR spectra of certain wavenumber regions of 25PhTMS (colors represent the Na-DES loading), NaTFSI (black), and Na-DES (NaTFSI/NMA) (grey). (a) 1740-1470 cm^{-1}, (b) 1400-1275 cm^{-1}, (e) 1265-965 cm^{-1}, and (f) 850-718 cm^{-1} (ν: vibration, as: asymmetric, ip: in-plane, oop: out-of-plane). (c) Chemical structure of the $TFSI^-$ anion. (d) Chemical structure of NMA. Solid-state NMR spectra of 25PhTMS (organically modified eutectogel) with different loadings. (g) ^{1}H-NMR spectra showing three peaks of NMA protons (number corresponds to the assigned protons in (d) and peaks at ~3.7 ppm belonging to H_2O (see SI, Figure S11). (h) ^{19}F-NMR spectra showing the peak of the CF_3 groups of $TFSI^-$ anions. Both ^{1}H- and ^{19}F-NMR spectra show narrower peaks upon increased DES-loading, meaning that the mobility of the DES molecules increases. (i) ^{23}Na-NMR spectra showing a single peak of the Na^+ ion, which becomes broader when the DES loading increases (less organized chemical environments).

Eutectogels (of the class 25PhTMS) with different DES loadings were studied with NMR spectroscopy to obtain more information about the interactions between the different chemical entities. The ^{1}H-NMR spectrum is dominated by the characteristic peaks of the DES (Figure 3g).[23] The downfield peak (6.70 ppm) relates to the proton on the NMA nitrogen atom. The peaks at 2.48 and 1.71 ppm relate to the protons of the methyl groups on the nitrogen atom and the alpha carbon, respectively. An additional peak is present around 3.7 ppm (most visible for 25PhTMS_4.00). To further investigate the origin of this peak, 25PhTMS_2.00 was spiked with water, which confirmed the presence of water in the unspiked eutectogel. The ^{1}H-NMR spectra of the spiked samples can be found in Figure S11. Water is one of the products formed during the condensation of the silica matrix.[41] Furthermore, the presence of hydrogen bond donors and acceptors on the NMA molecules makes the presence of water in the bulk of the DES very likely. As shown in our previous work, water hydrogen-bonded to the silica surface is not mobile enough to be visible in NMR, and so its presence cannot be excluded.[22] Based on the ^{1}H-NMR spectra, it is clear that increasing the eutectogel DES loading and, thus, increasing the number of NMA molecules, leads to the presence of more mobile water in the bulk of the DES. All eutectogels contain mobile water in the liquid DES despite the long drying time (> 50 days storage in a dry room). The ^{1}H-NMR peaks become narrower with increasing DES loading, indicating increased NMA molecule mobility. The same observation can be made in the

^{19}F-NMR spectra (Figure 3h). $TFSI^-$ anions are more mobile (narrower signal) in eutectogels with high DES loading. The single ^{19}F-NMR peak at -77.5 ppm corresponds to the fluorine atoms of the $TFSI^-$ anions and shows no change in chemical shift, and thus no change in the chemical environment, over the studied samples. This might suggest that H_2O does not strongly interact with $TFSI^-$ anions. The ^{23}Na-NMR spectra show one peak at -19.2 ppm, which shifts slightly to higher ppm values when more DES is present in the gels (Figure 3i). The increased chemical shift might be caused by the higher amount of H_2O inside the gel. Remarkably, the width of the ^{23}Na-NMR peak increases with DES loading, which contrasts with the peaks observed for NMA and $TFSI^-$ in the ^{1}H- and ^{19}F-NMR spectra. As was seen by ATR-FTIR, NaTFSI crystallizes to some extent in eutectogels with low DES loading. This results in an ordered Na^+ ion environment, creating sharper ^{23}Na-NMR peaks. With higher DES loadings (and thus more NMA and water), the Na^+ ions are partially hydrated. As such, eutectogels with different DES loadings have different conductivities not only because of different content of conducting liquid, but also because of a different coordination environment of the Na^+ ions. After all, the changing chemical shift of the Na^+ ions (and of the water peak in the ^{1}H-NMR spectra) suggests a strong interaction between the water molecules and the Na^+ ions. This hydration leads to more heterogeneity in the chemical environments of the Na^+ ions, resulting in ^{23}Na-NMR peak broadening. As no NaTFSI crystallization was observed with high DES loadings, the $TFSI^-$ anions are more mobile, which leads to sharper ^{19}F-NMR peaks. The ^{1}H-, ^{19}F-, and ^{23}Na-NMR of 100TEOS and 12.5DPhDMS samples, where similar observations can be made, can be found Figure S12 in the supporting information.

Summarizing the spectroscopic information presented above, an important difference between 25PhTMS_1.00 and 25PhTMS_4.00 is their amount of DES and water. A representation of the chemical interactions inside low-loaded (25PhTMS_1.00) and high-loaded (25PhTMS_4.00) eutectogels is given in Figure 4. Completely removing the coordinated water molecules during the drying stage is impossible, given the high number of possible hydrogen bonding sites. However, the presence of water inside the eutectogels does not necessarily pose a problem for their electrochemical performance, as can be inferred from their broad electrochemical stability windows (Figure 2, Figure S7). Other works studying the effect of the presence of water on the functional performance of DESs concluded that hydrogen bonding mitigates water's electrochemical activity.[27, 42] Therefore, we presume that the strong coordination of water in the eutectogels studied in the work at hand prevents its electrochemical activation and increases its stability toward oxidation and reduction. In eutectogels with lower DES loading, there is an increased interaction of NMA molecules with the silica matrix. Increasing the DES loading leads to more mobile water in the DES bulk, causing Na^+ ions to interact with water through ion-dipole interactions. As mentioned above, the ionic conductivity of organically modified eutectogels is slightly higher than the conductivity of eutectogels without organic modification, but with the same DES loading. This may be explained by hydrophobic phenyl groups driving the water molecules to the bulk DES and altering the coordination environment of the Na^+ ions.

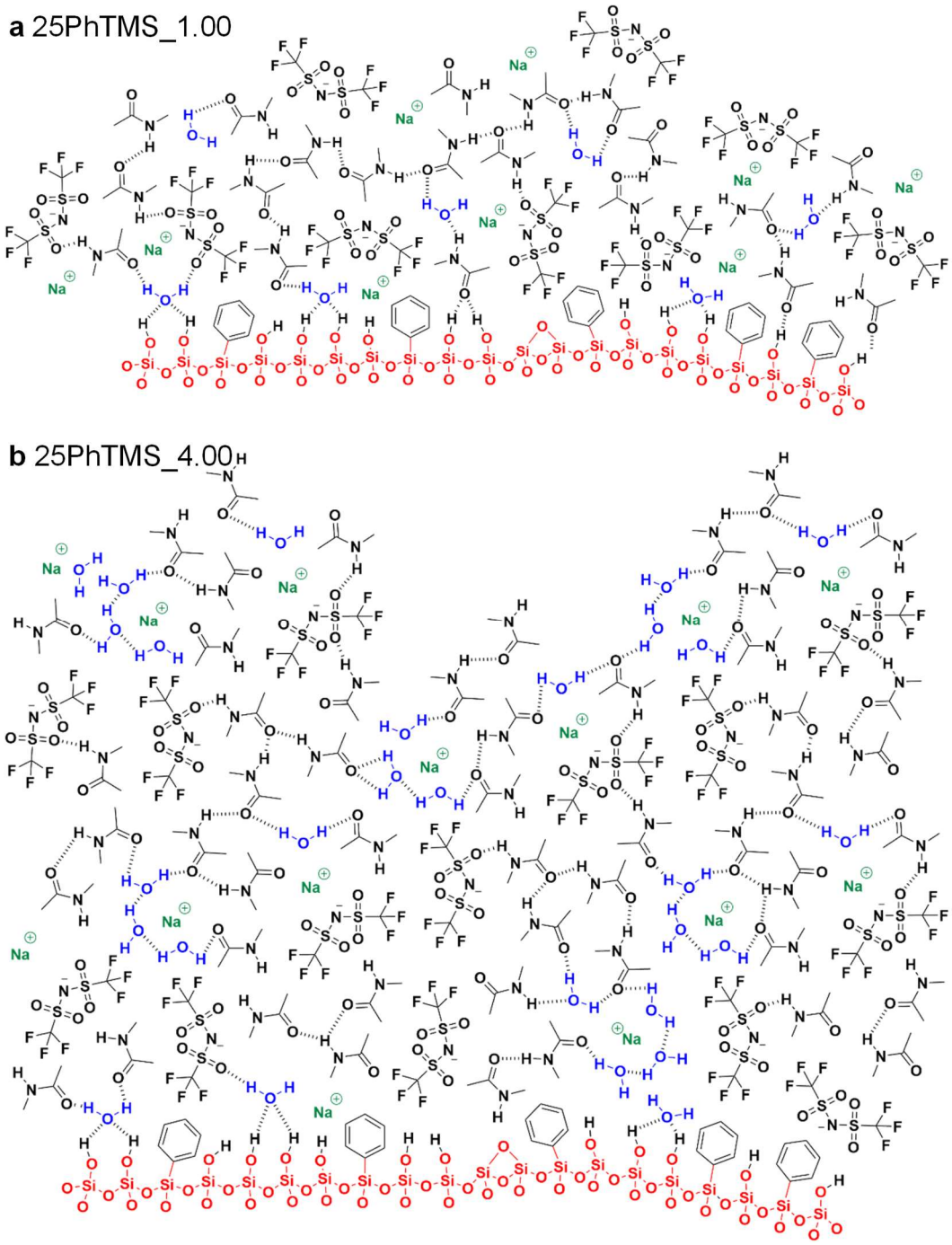

Figure 4. Possible interactions inside organically modified eutectogels based on the results of NMR, ATR-FTIR, and Raman spectroscopy. (a) Organically modified eutectogel with NMA/total Si = 1.00 (25PhTMS_1.00) and (b) Organically modified eutectogel with NMA/total Si = 4.00 (25PhTMS_4.00).

Electrochemical performance

To investigate the impact of organic modification on electrochemical performance, 100TEOS_4.00 and 25PhTMS_4.00 were investigated in full cells. After all, both eutectogels have a similar electrochemical stability window and ionic conductivity (0.16 and 0.17 mS cm^{-1} for 100TEOS_4.00 and 25PhTMS_4.00, respectively), but a considerably different Young's modulus (4.8 and 2.1 MPa, respectively). The full cells contained Prussian blue (PB) as active positive electrode material and carbon-coated $NaTi_2(PO_4)_3$ (C-NTP) as active negative electrode material. PB has a theoretical reversible capacity of 170 mAh g^{-1}, with a working potential of ~3.2 V versus Na^+/Na.[43] C-NTP has a theoretical capacity of 133 mAh g^{-1}, with a voltage plateau at 2.1 V versus Na^+/Na.[44, 45] The electrochemical performance of both electrodes in half cell configuration can be found in Figure S13.

Full cells containing (organically modified) eutectogels have a similar rate performance as full cells containing a conventional liquid electrolyte (Figure 5). Figure S13 gives the galvanostatic plots of the rate performance tests. The following discharge capacities were obtained in the final cycle (0.1 C): full cell with 1M $NaClO_4$ in EC:PC: 70 ±

3 mAh g^{-1}; DES: 60.0 ± 0.6 mAh g^{-1}; 100TEOS_4.00: 69 ± 5 mAh g^{-1}; and 25PhTMS_4.00: 74 ± 7 mAh g^{-1}. At 2 C, cells containing the DES as electrolyte deliver the highest capacity (13 mAh g^{-1}), presumably because the liquid can completely fill the electrode porosity, which is not possible for the investigated eutectogels. The cycle stability tests (0.2 C) of full cells containing various electrolyte compositions are shown in Figure S14. All cells show a large capacity fade during the first 50 cycles. The cycle life of the cells is presumed to be dominated by the loss of electrochemically active Na^+ ions over the course of cycling.[46, 47] At cycle 100, the following capacities are obtained: full cell with 1M $NaClO_4$ in EC:PC: 51.0 ± 0.1 mAh g^{-1}; DES: 53 ± 5 mAh g^{-1}; 100TEOS_4.00: 38 ± 5 mAh g^{-1}; and 25PhTMS_4.00: 36 ± 2 mAh g^{-1}. The best coulombic efficiencies (CEs) were obtained for the full cell with the DES as electrolyte (99.5% ± 0.1 at cycle 200). The standard electrolyte (1M $NaClO_4$ in EC/PC) induced the lowest CEs (98.5% ± 0.7 at cycle 200), presumably because of the occurrence of side reactions. The complete optimization of SIB full cells was beyond the scope of this study. EIS was used to investigate the evolution of the charge transfer resistance (R_{ct}) over the course of the cycle life tests (Figure 5), in an effort to obtain insight into the electrolyte-electrode contacts. The corresponding EIS spectra can be found in Figure S15. Only negligible changes in R_{ct} can be observed over the course of the 16 hour OCV period after cell assembly, confirming the (electro)chemical stability of the eutectogels toward the electrodes (PB and C-NTP). R_{ct} slightly increases over the course of cycling, indicating the formation of degradation layers on the electrode surfaces. The R_{ct} values of cells containing 25PhTMS_4.00 are consistently lower than those of cells containing 100TEOS_4.00 as electrolyte. We attribute this difference to their different mechanical properties: 25PhTMS_4.00 (2.1 MPa) has a lower Young's modulus than 100TEOS_4.00 (4.8 MPa), indicating that the former is more ductile and more easily adapts to rough electrode surfaces. This translates into better electrode/electrolyte contact and lower R_{ct} values.

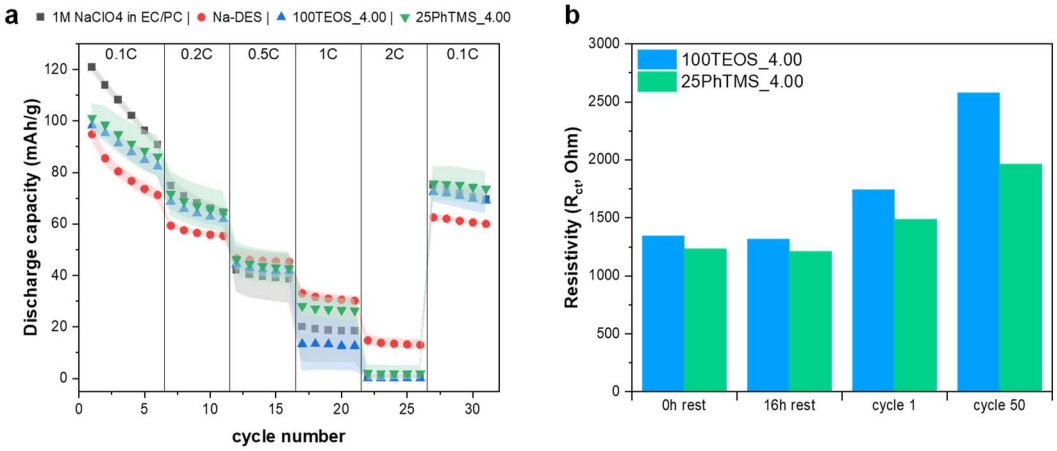

Figure 5. (a) Rate capability test of C-NTP|electrolyte|PB full cells with 1M $NaClO_4$ in EC:PC, Na-DES, 100TEOS_4.00, and 25PhTMS_4.00 as electrolyte. Shaded areas indicate the standard deviation between three separate measurements. (b) Charge transfer resistances remain constant during the rest period and tend to increase during cycling. 25PhTMS_4.00 has lower R_{ct} values compared to 100TEOS_4.00, in accordance with their Young's moduli. EIS was measured at 0 and 16 h after assembly and after cycle 1 and 50 of PB|eutectogel|C-NTP full cells with 100TEOS_4.00 and 25PhTMS_4.00 as eutectogel (electrolyte). The PB electrodes had an average loading of ~1.9 mg cm^{-2} and the C-NTP electrodes had an average loading of ~2.5 mg cm^{-2}. The N/P ratio was 1.1. The tests were performed at room temperature.

Comparison with State-of-the-Art electrolytes

A comparison of organically modified eutectogels with other solid/gel electrolytes for SIBs, based on the work of Zhao *et al.*, is given in Figure 6.[48] Inorganic solid electrolytes, such as Na-β-Al_2O_3 and NASICON, generally suffer from poor ionic conductivity. Further, their high interfacial resistance is one of the most important concerns related to this type of electrolyte. This is also the case for sulfide-based solid electrolytes (such as Na_3PS_4), even if they can reach high ionic conductivity values (from 4.17 x 10^{-6} to 2.3 x 10^{-4} S cm^{-1}). Gel-polymer electrolytes (GPEs) are closely related to eutectogels, but their solid matrix is a polymer (polyethylene oxide, PEO) and the liquid is an ILE. As such, GPEs have similar functional properties (conductivity of ~2 x 10^{-3} S cm^{-1}, ESW of ~4 V) as organically modified eutectogels. Still, the silica-based solid host structure of the latter endows them with an enhanced thermal stability compared to GPEs. Finally, solid polymer electrolytes (SPEs), often based on PEO, have the advantage of a reduced interfacial resistance, but suffer from low ionic conductivities (< 10^{-6} S cm^{-1} at room temperature). Furthermore, the ESW of SPEs depends significantly on the polymer (and can be as low as ~2.7 V).[48] From this comparison, it is clear that the organically modified eutectogels discussed in the paper at hand can be a viable electrolyte for future SIBs.

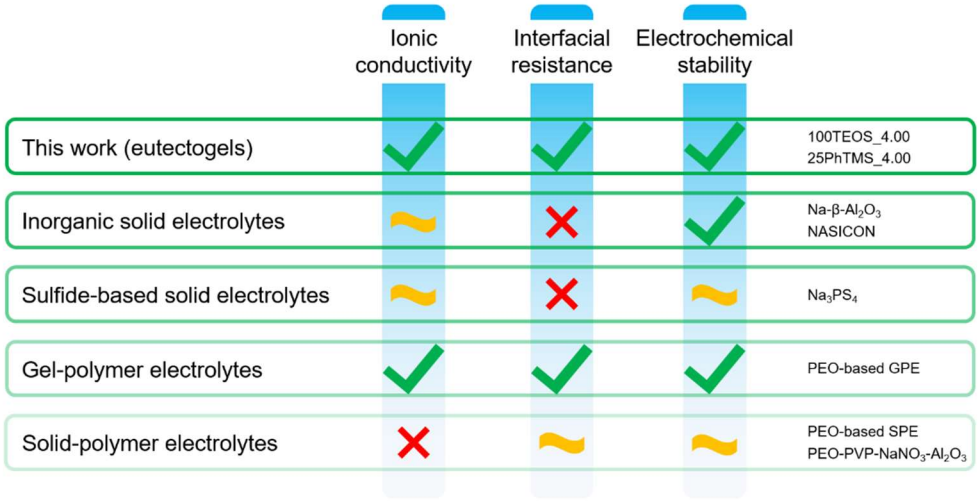

Figure 6. Comparison organically modified eutectogels with other classes of solid/gel electrolytes used in SIBs according to their properties.

Conclusion

This study reports a series Na^+ ion conducting eutectogels, consisting of a DES encapsulated within a silica matrix which was organically modified by introducing phenyl moieties. In contrast to previously reported ionogels, organic modification positively affected their ionic conductivity, reaching values up to 0.171 mS cm^{-1}. The electrochemical stability window of the eutectogels was completely determined by the DES, reaching from ~1.0 V vs. Na^+/Na to ~4.5 vs. Na^+/Na. This implies that the water in the eutectogels – of which the presence was proven using several spectroscopic techniques – does not affect their electrochemical stability, even if water was determined to coordinate to Na^+ ions in eutectogels with high DES loading. Increasing extents of organic modification consistently decreased the Young's modulus of the eutectogels (down to 2.1 MPa), resulting in more ductile materials. SIB full cells containing eutectogels had a similar rate performance as cells containing a liquid electrolyte. Using eutectogels with a higher extent of organic modification mitigated the increase in charge transfer resistance over the course of cycling. This indicates that organic modification is a successful strategy for improving electrode/electrolyte contact in solid-state SIBs, owing to the resulting increase in ductility. As such, organic modification can simultaneously improve ionic conductivity and electrode/electrolyte contact in eutectogels, providing new opportunities for the further development of solid and gel electrolytes for SIBs.

Experimental

Chemicals. Sodium bis(trifluoromethanesulfonyl)imide (NaTFSI, 99.5%) was purchased from Solvionic (France). *N*-methyl acetamide (NMA, ≥99%) was purchased from Sigma-Aldrich (Belgium). Formic acid (FA, 98%+) was purchased from Thermo Scientific (Belgium). Tetraethylorthosilicate (TEOS, 98%), phenyltrimethoxysilane (PhTMS, 97%), and diphenyldimethoxysilane (DPhDMS, 97%) were purchased from Alfa Aesar (Thermo Scientific, Belgium). The materials used for coin cell preparation were carbon black (C-Nergy™ Super C65) purchased from Imerys (France), *N*-methyl pyrrolidone (NMP, ≥99.8%) purchased from Carl Roth (Belgium), alginic acid sodium salt purchased from Alfa Aesar (Thermo Scientific, Belgium), carbon-coated $NaTi_2(PO_4)_3$ (C-NTP), and Prussian Blue (PB, $Na_{0.61}Fe[Fe(CN)_6]_{0.94}$) purchased from NEI Corporation (USA). All chemicals were used as received.

Synthesis of the deep eutectic solvent and organically modified eutectogels. The DES used in this study, NaTFSI dissolved in *N*-methyl acetamide (NMA) in a 3/7 molar ratio was chosen based on the work of De Sloovere *et al*.[23] The 5.86 molal DES was prepared in an Ar-filled glovebox (Sylatech, humidity < 1.0 ppm, O_2 < 0.6 ppm) by dissolving 2.500 g NaTFSI in 1.406 g melted NMA (at 40 °C). The solution was stirred at room temperature for at least 16 hours to dissolve the NaTFSI salt completely. The solution was kept inside the glovebox until further use. The chemicals were not dried before use: as there is in-situ formation of H_2O during the condensation of the silica matrix in the eutectogels, this would have been redundant (**Error! Reference source not found.**). Monoliths of the organically modified eutectogels were synthesized based on a procedure for organically modified ionogels.[22] The sample compositions and examples of the volumes and masses used to prepare 100TEOS_1.00, 25PhTMS_1.00, and 12.5DPhDMS_1.00 can be found in Table 2 and Table S1. A desired amount of DES was taken from the glovebox, followed by the addition (volumetric pipet with piston) of formic acid (FA) to the DES in ambient atmosphere. The mixture was stirred in a closed vial for 5 minutes. Afterward, depending on the amount of organic modification, PhTMS or DPhDMS, and TEOS were consecutively added and left to stir in a closed vial for 5 minutes at room temperature. The transparent solutions were transferred into custom-made Teflon molds

using a syringe with a needle to avoid air bubbles inside the molds. A photograph of the molds can be found in our previous study.[22] The molds containing the precursor solution were then left to gel for 48 hours at room temperature in normal lab ambient and aged for 5 days at 45 °C and 10.0% relative humidity in a climate chamber (Memmert GmbH & Co., ICH110). After the gelation and aging periods, the gels were carefully removed from the molds and transferred to a dry room (relative humidity <0.5 %). Each gel was dried for at least 50 days in a plastic case with a hole of 2 mm diameter to slow the drying process (**Error! Reference source not found.**). The eutectogels were also synthesized inside glass fiber (GF) separators (EL-Cell) for electrochemical characterization and coin cell tests. The synthesis is similar to the synthesis of the eutectogel monoliths. Here, the precursor solutions are not injected into molds, but GF separators are soaked with the precursor solutions and left to gel on a Teflon plate for 5 days in ambient atmosphere. During the gelation, the gels were covered. Additional drying was done in a dry room for at least 50 days (relative humidity <0.5 %) in a plastic case with two 2 mm diameter holes (**Error! Reference source not found.**).

Mechanical analysis. Compression testing was performed on a Shimadzu AGS-X mechanical analyzer tester with a 500 N load cell at room temperature. Monoliths of the organically modified eutectogels were compressed between two stainless steel plates at a rate of 1 mm min^{-1}. The Young's modulus (*E*) was calculated as the slope of the stress-strain curve for a strain below 25%. At least three dried samples per composition were measured to obtain a standard deviation on the results. Measurements were carried out after exposing the dried samples to the ambient atmosphere for less than 4 hours.

Physicochemical properties. The thermal stability was analyzed with a TA Instruments Q500 thermogravimetric analyzer (TGA) equipped with a ceramic oven. Measurements were conducted in dry air atmosphere (60 mL min^{-1}). Samples of ~5 mg were kept isothermal at 25 °C for 30 minutes before being heated to 750 °C at a heating rate of 10 °C min^{-1}. A TA Instruments Q200 differential scanning calorimeter (DSC) was used to analyze samples (~2-5 mg) in aluminum hermetic pans from -90 °C to 70 °C at 10 °C min^{-1} for 3 cycles under a nitrogen flow of 50 mL min^{-1}. Sample preparation was performed in a dry room. A Perkin Elmer Frontier Fourier-transform infrared spectrometer equipped with a Pike MIRacle single reflection attenuated total reflectance (ATR) accessory was used to characterize the samples. The scan range was 4000-600 cm^{-1} with a resolution of 2 cm^{-1} for 8 scans. The spectra were normalized. Raman spectra were collected using a Renishaw InVia Qontor Confocal Raman Microscope with a 100x objective lens and a 532 nm excitation wavelength (100 mW) to give a laser spot diameter of approximately 1 µm. The Raman shift scale was calibrated using silicon. The measurements were performed at RT in a continuous scan mode (SynchroScan) with an exposure time of 10 s, 2 accumulations, 50% laser power, and using a 2400 l mm^{-1} grating. The dried samples were prepared in a dry room by placing them between glass plates sealed with vacuum grease to protect them from ambient air. The obtained spectra were analyzed using Renishaw WIRE 5.5 software and normalized. The background and cosmic rays were removed when present. High-resolution solid-state MAS (magic angle spinning) NMR spectra were acquired at ambient temperature on an Agilent VNMRS DirectDrive 400 MHz spectrometer (9.4 T wide bore magnet) equipped with a T3HX 3.2 mm probe. MAS was performed at 6 kHz using 3.2 mm zirconia rotors (22 µL rotors). The resonance frequencies were 399.96, 376.34, and 105.80 MHz for ^{1}H-, ^{19}F- and ^{23}Na-NMR, respectively. Acquisition parameters used were i) for ^{1}H-NMR: a spectral width of 208 kHz, a 90° pulse length of 2 µs, an acquisition time of 80 ms, a recycle delay time of 10 s and 16 accumulations; ii) for ^{19}F-NMR: a spectral width of 208 kHz, a 30° pulse length of 20 µs, an acquisition time of 24 ms, a recycle delay time of 2 s and 16 accumulations; and iii) for ^{23}Na-NMR: a spectral width of 78 kHz, a 90° pulse length of 2.5 µs, and acquisition of 30 ms, a recycle delay time of 3 s and 200 accumulations.

Electrochemical characterization. The ionic conductivities of dried monolithic organically modified eutectogels were measured with electrochemical impedance spectroscopy (EIS) and calculated based on the intercept of the EIS with the real axis. The open circuit potential (OCP) was perturbed with an amplitude of 10 mV over a frequency range from 7 MHz to 1 Hz at room temperature and in the temperature range of -10-60 °C with a Bio-Logic SP-300 potentiostat. The eutectogels were analyzed between two stainless steel plates, and the thickness was measured with a digital micrometer. Additional experimental details can be found in our previous work.[22] Fitting parameters of the ionic conductivity in function of temperature were determined using OriginPro (See SI, **Error! Reference source not found.**). Linear sweep voltammetry (LSV) was measured using a three-electrode set-up (El-Cell ECC-REF) with Na metal as a reference and counter electrode and a stainless steel plate as the working electrode. The cell potential was increased from OCP to 7 V or decreased from OCP to -1 V vs Na^{+}/Na at 1 mV s^{-1} after a resting period of two hours. The electrochemical compatibility of the eutectogels against Na metal and electrode materials was tested by EIS in a symmetric electrode|eutectogel|electrode cell. EIS (Bio-Logic, VMP-3) was performed by perturbing the OCP with an AC sinusoidal potential of 10 mV amplitude over 10 kHz - 100 mHz every 60 minutes.

C-coated $NaTi_2(PO_4)_3$ (C-NTP) || Prussian blue (PB) full cells. C-NTP ($Q_{theoretical}$: 133 mAh g^{-1}) and PB ($Q_{theoretical}$: 170 mAh g^{-1}) electrode slurries (1 g) were prepared with 85 wt% active material, 10 wt% total carbon, and 5 wt% binder. The total carbon for C-NTP coatings equals carbon black and the carbon originating from the 3 wt% carbon-coating on NTP. The total carbon for PB coatings equals the carbon black. A 1.5 wt% Na-alginate solution in milli-

Q water was used as binder solution for the C-NTP electrode. A 1.3 wt% PVDF (polyvinylidene fluoride) in NMP solution was used as a binder and solvent for the PB electrode. The components were mixed by ball milling (Retsch Emax, 500 rpm, 30 minutes, 5 x 1 cm zirconia balls). The C-NTP slurry was coated on 10 µm thick copper foil (blade height: 120-140 µm), whereas the PB slurry was coated on 15 µm thick aluminum foil (blade height: ~125 µm). The coated slurries were dried at 60 °C in an oven overnight. Punches, 15 mm in diameter, were further dried for 16 h under vacuum at 110 °C (Buchi glass oven B-585) before insertion in the glovebox (MBraun, H_2O < 0.6 ppm, O_2 < 0.1 ppm). A ~2.5 mg cm^{-2} mass loading for the C-NTP electrode and a ~1.9 mg cm^{-2} mass loading for the PB electrode were obtained. Before full cell assembly, the PB electrode punches were completely discharged in Na half cells with 1M $NaClO_4$ in EC/PC as the electrolyte and cleaned with DMC (discharged from OCP to 2.2 V at 0.05 C). Full cells with ~10% excess anode active material capacity were assembled in an Ar-filled glovebox (MBraun, H_2O < 0.6 ppm, O_2 < 0.1 ppm). The eutectogels prepared in GF separators were used as the electrolyte in the coin cells. The full cell rate performance (0.01-2.3 V) was tested after a 16 hour OCP period, at 0.1, 0.2, 0.5, 1, 2, and 0.1 C for 5 cycles at room temperature. Cycle life (NEWARE BT-4008) was tested at 0.2 C for 200 cycles at room temperature. Charge-transfer resistances (R_{ct}) were determined by cycling half cells at 0.2 C intermittently recording an EIS (10 mV amplitude over 10 kHz - 100 mHz). This was done at directly after assembly, after a 16 h OCP period, and after the first cycle. Thereafter EIS was recorded every 5 cycles (Bio-Logic BCS-805).

Supporting Information

The authors have cited additional references within the Supporting Information.[49-53]

Acknowledgements

This research was made possible by the Research Foundation Flanders (FWO, project G053519N and 1S08921N) and the Special Research Fund (BOF) of Hasselt University (BOF20INCENT19). This work was further supported by Hasselt University and FWO Vlaanderen via the Hercules projects AUHL/15/2-GOH3816N and I001324N.

Keywords: Conductivity • Electrochemistry • Organic-inorganic hybrid composites • Phenyl • Young's modulus

[1] A. King. Northvolt to bring sodium-ion batteries to European market. 2023 10/04/2024; Available from https://www.chemistryworld.com/news/northvolt-to-bring-sodium-ion-batteries-to-european-market/4018576.article.

[2] S. Siddiqi. Sodium-Ion Batteries: From Research to Commercialisation. 2023 11/04/2024; Available from: https://www.idtechex.com/en/research-article/sodium-ion-batteries-from-research-to-commercialization/29115.

[3] M. Baumann, M. Häringer, M. Schmidt, L. Schneider, J. F. Peters, W. Bauer, J. R. Binder, M. Weil, Advanced Energy Materials 2022, 12, 2202636.

[4] S. Hanley. CATL Reveals Sodium-Ion Battery With 160 Wh/kg Energy Density. 2021 11/04/2024; Available from: https://cleantechnica.com/2021/07/30/catl-reveals-sodium-ion-battery-with-160-wh-kg-energy-density/.

[5] V. Henze. Lithium-ion Battery Pack Prices Rise for First Time to and Average of $151/kWh. 2022 11/04/2024; Available from: https://about.bnef.com/blog/lithium-ion-battery-pack-prices-rise-for-first-time-to-an-average-of-151-kwh/.

[6] Krampf, S. Sodium Batteries to Disrupt Energy Storage Market by 2027. 2024 [cited February 18, 2025]; Available from: https://sodiumbatteryhub.com/2024/07/01/sodium-batteries-to-disrupt-energy-storage-market-by-2027/.

[7] K. Chayambuka, G. Mulder, D. L. Danilov, P. H. Notten, Advanced energy materials 2020, 10, 2001310.

[8] Mineral Commodity summaries 2024, in Mineral Commodity Summaries, National Minerals Information Center, 2024.

[9] Sustainable. And attainable.[11/04/2024]; Available from: https://northvolt.com/products/cells/sodium-ion/.

[10] Reid, M. Sodium-ion batteries: disrupt and conquer? 2023 February 21, 2023 October 22, 2024]; Available from: https://www.woodmac.com/news/opinion/sodium-ion-batteries-disrupt/.

[11] J. Deng, C. Bae, A. Denlinger, T. Miller, Joule 2020.

[12] CATL Unveils Its Latest Breakthrough Technology by Releasing Its First Generation of Sodium-ion Batteries. 2021 July 29, 2021 October 22, 2024]; Available from: https://www.catl.com/en/news/665.html.

[13] N. Aslfattahi, L. Samylingam, M. S. Kiai, K. Kadirgama, V. Kulish, M. Schmirler, Z. Said, Journal of Energy Storage 2023, 72, 108781.

[14] S. Kainat, J. Anwer, A. Hamid, N. Gull, S. M. Khan, Materials Chemistry and Physics 2023, 128796.

[15] Q. Zhao, S. Stalin, C.-Z. Zhao, L. A. Archer, Nature Reviews Materials 2020, 5, 229.

[16] G. G. Eshetu, G. A. Elia, M. Armand, M. Forsyth, S. Komaba, T. Rojo, S. Passerini, Advanced Energy Materials 2020, 10, 2000093.

[17] W. J. Hyun, C. M. Thomas, M. C. Hersam, Advanced Energy Materials 2020, 10, 2002135.

[18] X. Fan, S. Liu, Z. Jia, J. J. Koh, J. C. C. Yeo, C.-G. Wang, N. E. Surat'Man, X. J. Loh, J. Le Bideau, C. He, Chemical Society Reviews 2023.

[19] E. L. Smith, A. P. Abbott, K. S. Ryder, Chemical reviews 2014, 114, 11060.

[20] B. Joos, T. Vranken, W. Marchal, M. Safari, M. K. Van Bael, A. T. Hardy, Chemistry of Materials 2018, 30, 655.

[21] B. Joos, J. Volders, R. R. da Cruz, E. Baeten, M. Safari, M. K. Van Bael, A. T. Hardy, Chemistry of Materials 2020, 32, 3783.

[22] J. Mercken, D. De Sloovere, B. Joos, L. Calvi, G. Mangione, L. Pitet, E. Derveaux, P. Adriaensens, M. K. Van Bael, A. Hardy, Small 2023.

[23] D. De Sloovere, D. E. P. Vanpoucke, A. Paulus, B. Joos, L. Calvi, T. Vranken, G. Reekmans, P. Adriaensens, N. Eshraghi, A. Mahmoud, F. Boschini, M. Safari, M. K. Van Bael, A. Hardy, Advanced Energy and Sustainability Research 2022, 2100159

[24] A.-S. Kelchtermans, D. De Sloovere, J. Mercken, T. Vranken, G. Mangione, B. Joos, W. Vercruysse, D. Vandamme, H. Hamed, M. Safari, ACS omega 2024, 9, 42343.

[25] M. J. Panzer, Materials Advances 2022, 3, 7709.

[26] J. Wang, S. Zhang, Z. Ma, L. Yan, Green Chemical Engineering 2021, 2, 359.

[27] T. Liu, H. Wu, X. Du, J. Wang, Z. Chen, H. Wang, J. Sun, J. Zhang, J. Niu, L. Yao, ACS Applied Materials & Interfaces 2022, 14, 33041.

[28] M. Uhl, T. Geng, P. A. Schuster, B. W. Schick, M. Kruck, A. Fuoss, A. J. Kuehne, T. Jacob, Angewandte Chemie International Edition 2023, 62, e202214927

[29] M. Uhl, Sadeeda, P. Penert, P. A. Schuster, B. W. Schick, S. Muench, A. Farkas, U. S. Schubert, B. Esser, A. J. Kuehne, ChemSusChem 2024, 17, e202301057.

[30] W. Xiong, X. Zhang, Z. Tu, X. Hu, Y. Wu, Industrial & Engineering Chemistry Research 2022, 62, 51.

[31] J. Chidiac, G. Nikiforidis, L. Timperman, M. Anouti, ChemPhysChem 2022, 23, e202200224.

[32] H. Yang, Y. Qi, Z. Wang, Q. Pan, C. Zhang, J. Yan, K. Cen, Z. Bo, K. Ostrikov, Energy & Environmental Materials 2023, e12641.

[33] G. Tan, F. Wu, C. Zhan, J. Wang, D. Mu, J. Lu, K. Amine, Nano Letters 2016, 16, 1960

[34] F. Wu, N. Chen, R. Chen, L. Wang, L. Li, Nano Energy 2017, 31, 9.

[35] Y. Wu, Y. Xu, D. Wang, Y. Zhao, S. Weng, D. Xu, J. Wu, Journal of applied polymer science 2004, 91, 2869

[36] M. Hernandez, L. Servant, J. Grondin, J. Lassegues, Ionics 1995, 1, 454.

[37] J. Kubelka, T. A. Keiderling, The Journal of Physical Chemistry A 2001, 105, 10922

[38] Y. Hu, Z. Wang, H. Li, X. Huang, L. Chen, Spectrochimica Acta Part A: Molecular and Biomolecular Spectroscopy 2005, 61, 2009.

[39] J.-C. Lassègues, J. Grondin, C. Aupetit, P. Johansson, The Journal of Physical Chemistry A 2009, 113, 305

[40] I. Rey, P. Johansson, J. Lindgren, J. Lassegues, J. Grondin, L. Servant, The Journal of Physical Chemistry A 1998, 102, 3249.

[41] K. G. Sharp, Journal of Sol-Gel Science and Technology 1994, 2, 35.

[42] X. Hou, T. P. Pollard, X. He, L. Du, X. Ju, W. Zhao, M. Li, J. Wang, E. Paillard, H. Lin, Advanced Energy Materials 2022, 12, 2200401.

[43] Y. Yue, A. J. Binder, B. Guo, Z. Zhang, Z. A. Qiao, C. Tian, S. Dai, Angewandte Chemie International Edition 2014, 53, 3134.

[44] S. Chen, C. Wu, L. Shen, C. Zhu, Y. Huang, K. Xi, J. Maier, Y. Yu, Advanced Materials 2017, 29, 1700431

[45] M. Wu, W. Ni, J. Hu, J. Ma, Nano-Micro Letters 2019, 11, 1.

[46] Y. Pi, Z. Gan, M. Yan, C. Pei, H. Yu, Y. Ge, Q. An, L. Mai, Chemical Engineering Journal 2021, 413, 127565

[47] X. Chen, Y. Zheng, W. Liu, C. Zhang, S. Li, J. Li, Nanoscale 2019, 11, 22196.

[48] S. Zhao, H. Che, S. Chen, H. Tao, J. Liao, X.-2. Liao, Z.-F. Ma, Electrochemical Energy Reviews 2024, 7, 3.

[49] A. Alhadid, L. Mokrushina, M. Minceva, Journal of Molecular Liquids 2020, 314, 113667.

[50] Y. Ji, X. Yang, Z. Ji, L. Zhu, N. Ma, D. Chen, X. Jia, J. Tang, Y. Cao, ACS omega 2020, 5, 8572.

[51] Larkin, P.J., Illustrated IR and Raman Spectra Demonstrating Important Functional Groups. 2018, Elsevier. p. 153-210.

[52] A. V. Rao, R. R. Kalesh, G. Pajonk, Journal of Materials Science 2003, 38, 4407.

[53] L. B. Capeletti, I. M. Baibich, I. S. Butler, J. H. dos Santos, Spectrochimica Acta Part A: Molecular and Biomolecular Spectroscopy 2014, 133, 619.